RSC Advances

PAPER

View Article Online
View Journal | View Issue

Cite this: *RSC Adv.*, 2017, **7**, 25549

Substituent-tuned structure and luminescence sensitizing towards Al^{3+} based on phenoxy bridged dinuclear Eu^{III} complexes†

Jing-Jing Zhou, Xue-Qin Song,* Yuan-Ang liu and Xiao-Long Wang

To develop a Ln^{III} complex-supported chemsensor, two new phenoxy bridged dinuclear Eu^{III} complexes, $[Eu_2(H_2L)_3(NO_3)_3]\cdot 3CH_3CN$ (EuL) and $[Eu_2(H_2L')_2(NO_3)_4]\cdot 3CH_3CN$ (EuL′), constructed by two new structurally related salicylamide salen-like ligands, 1-(2-hydroxy-benzamido)-2-(2-hydroxy-5-nitro-benzylideneamino)-ethane (H_3L) and 1-(2-hydroxy-benzamido)-2-(2-hydroxy-4-diethylamino-benzylideneamino)-ethane (H_3L'), have been synthesized and structural analysis shows that the different substitution groups on 2-(iminomethyl)phenol moiety have significant effects on their structures. Upon excitation of the ligand-centered absorption band at 375 nm, emissions both originating from ligands and Eu^{III} ions were observed in the two Eu^{III} compounds with the Eu^{III}-centered emission intensity more than three times higher than that of ligand-centered emission. The capability of EuL and EuL′ for selective detection Al^{3+} ions were evaluated and the results indicate EuL exhibits a turn-on luminescent enhancement as high as 5.7 fold with $K_d = 1.53 \times 10^{-4}$ in CH_3CN, but comparable compound EuL′ could not detect Al^{3+} among various cations. The considerably 'turn-on' luminescence response of EuL concomitantly led to the apparent color change from reddish to brilliant red, which could also be identified by naked eyes easily under UV lamp. This luminescence enhanced response can be explained in terms of the decrease of non-radiative transitions in EuL in addition to excited-state intra-molecular proton transfer (ESIPT) and photo-induced electron transfer suppression upon Al^{3+} coordination which is also rationalized by a theoretical calculation.

Received 26th February 2017
Accepted 29th April 2017

DOI: 10.1039/c7ra02386c

rsc.li/rsc-advances

1 Introduction

Luminescent lanthanide complexes display unrivalled spectroscopic properties, which place them in a special category in the luminescent toolbox. The attractive luminescence properties, especially, their characteristic line-like sharp emission bands which are unaffected by the Ln^{III} coordination environment make Ln^{III} luminescence appealing for a broad range of practical applications such as bioanalysis and biological imaging,[1] light conversion devices,[2] display materials,[3] and luminescent probes.[4] Since most of these f → f transitions are forbidden by the Laporte rule, the direct excitation of luminescent lanthanide(III) cations is inefficient. However, this limitation can be overcomed with the help of a highly absorbing "antenna" located in a sufficiently close proximity to the Ln^{III}.[5] Once a Ln^{III}-centred excited state has been reached *via* the antenna effect, the rules for radiative de-excitation are the same and the probability is weak. As a consequence, the excited-state lifetimes of Ln^{III} can be extremely long, up to a few milliseconds for visible Eu^{III} and Tb^{III} emitters.

Aluminum, a group 3 metal, is the third most abundant metal element in the crust of the earth, accounting for approximately 8% of its mass. It is well-known that aluminum is extensively used in our daily life and is also one important metal element applied in industry production. However, Al^{3+} is toxic and environmentally harmful. Due to the frequent use of aluminum vessels and foil, the risk of Al^{3+} ions absorption by the human body is increasing. For example, the iron-binding protein can carry Al^{3+} ions to the brain, which can further hurt the central nervous system. Al^{3+} has been implicated as the fatal factor in Alzheimer's disease, and it also prevents plant growth on acid grounds. The World Health Organization (WHO) prescribed the average human intake of aluminium is about 3–10 mg per day with a weekly dietary intake of 7 mg per day bodyweight.[6] Thus, it is urgent for development of selective and sensitive Al^{3+} chemsensors. Up to now, some fluorescent chemosensors have been designed for detection of Al^{3+}.[7] However, the fluorescence lifetimes of typical organic compounds,

School of Chemical and Biological Engineering, Lanzhou Jiaotong University, Lanzhou, China. E-mail: songxq@mail.lzjtu.cn; Fax: +86-0931-4938755; Tel: +86-0931-4938755

† Electronic supplementary information (ESI) available: A brief statement in CIF files, coordination polyhedron of EuL and EuL′ (Fig. S1 and S2), Job's plot between EuL and Al^{3+} (Fig. S3), ESI-MS spectra of EuL·Al (Fig. S4) and LOD curves (Fig. S5). CCDC 1534744 and 1534745. For ESI and crystallographic data in CIF or other electronic format see DOI: 10.1039/c7ra02386c

including common aluminum-selective fluorescent sensor molecules, are in the nanosecond region. On the other hand, among numerous sensors, luminescent lanthanide complexes, in particular Eu^{III} and Tb^{III} complexes receiving enormous interest due to their excellent optical properties in aid of an "antenna effect", such as large Stokes shifts and high color purity. An efficient strategy to prepare lanthanide complexes for detecting metal ion is to use lanthanide compounds with nonbonded functional ligand sites, where the lanthanide compounds provides luminescence, and the nonbonded functional sites interact with the metal ions. However, immobilization of functional site within the lanthanide compounds has been challenging due to their high reactivity during the synthesis. Up to now, only a few investigations on Ln^{III} complex based chemsensors with luminescence enhancement have been carried out to detect Zn^{2+},[8] Ag^{+},[9] K^{+},[10] as well as some anions.[11] These chemosensors were designed profiting from an analyte-induced alteration of antenna, shortening distance between the antenna and Ln^{III} or ligand exchange in solution. To our best knowledge, chemosensors based on Ln^{III} complexes are unprecedented for Al^{3+} because of the poor coordination ability and strong hydration aptitude of Al^{3+}. Inspired by these cases together with a continuation of our interest in the design of luminescent Ln^{III} complexes,[12] we dedicate to develop a chemsensor based on Ln^{III} complexes of salicylamide salen-like ligands by ingenious ligand design. Considering nitryl and diethamino group possess weaker binding abilities toward metal atoms than imine and amide group, when it situated within a highly electron-rich conjugate system, the lone pair electrons of N atoms can be spread and thereby realize the effective transfer of electrons and further influence the optical properties through environmental perturbation. Therefore, introduction of nitryl or diethylamino into salen-like salicylamide ligands may be a highly promising platform for construction of luminescent lanthanide chemsensor. We expect that metal ion binding to unoccupied coordination site of a Ln^{III} complex constructed by the salicylamide salen-like ligand would be conducive to a large luminescent response through the modulation of the sensitization process. Therefore, in this contribution, two new phenoxy bridged dinuclear Eu^{III} compounds, $[Eu_2(H_2L)_3(NO_3)_3]\cdot 3CH_3CN$ (EuL) and $[Eu_2(H_2L')_2(NO_3)_4]\cdot 2CH_3CN$ (EuL′) based on two structurally related salicylamide salen-like ligands were prepared by solvent evaporation method. Both the structural and luminescent investigations revealed that the different push–pull electronic substitution group on 2-(iminomethyl)phenol moiety of the salicylamide salen-like ligands have significant effect on their structures as well as luminescence responses toward Al^{3+}. We found that EuL exhibits a turn-on luminescent enhancement as high as 5.7 fold with $K_d = 1.53 \times 10^{-4}$ in CH_3CN, but comparable compound EuL′ could not detect Al^{3+} under the same experimental conditions. To the best of our knowledge, EuL is the first luminescence-enhanced Eu^{III} complex-supported Al^{3+} sensor. The sensing mechanism is presumably due to the formation of EuL·Al which result in effective suppression of non-radiative transitions, excited-state intra-molecular proton transfer (ESIPT) and photo induced electron transfer.

2 Experimental

2.1 Materials and physical measurements

Carbon, nitrogen and hydrogen analyses were performed using an EL elemental analyzer. Melting point were determined on a Kofler apparatus. ^{1}H NMR spectra of the ligands were recorded in d_6-DMSO solution at room temperature on a Bruker 400 instrument operating at a frequency of 400 MHz and referenced to tetramethylsilane (0.00 ppm) as an internal standard. Chemical shift multiplicities are reported as s = singlet, d = doublet, t = triplet and m = multiplet. Infrared spectra were obtained with KBr discs on a Nicolet FT-170SX instrument in the wavenumber range of 4000–400 cm^{-1} with an average of 128 scans and 4 cm^{-1} of spectral resolution. ESI-MS were determined on a HRMS spectrometer (model: QTOF Micro YA263). UV-vis absorption spectra were determined with a Varian UV-Cary100 spectrophotometer. Luminescence spectra were recorded on a F-7000 fluorescence spectrophotometer (Japan Hitachi company) at room temperature. The lifetime and quantum yield were measured at room temperature on FLS920 Steady State &Time-resolved fluorescence Spectrometer (Edinburgh Instrument).

2.2 Synthesis of the ligand

The synthesis of 1-(2-hydroxy-benzamido)-2-(2-hydroxy-5-nitro-benzylideneamino)-ethane (H_3L) and 1-(2-hydroxy-benzamido)-2-(2-hydroxy-4-diethylamino-benzylideneamino)-ethane (H_3L') are according to literature[13] with minor modification and using 2-hydroxy-5-nitrobenzaldehyde and 2-hydroxy-4-diethylaminobenzaldehyde instead (Scheme 1).

H_3L. Yellow solid. Mp 212–213 °C. Analytical data, calc. for $C_{16}H_{15}N_3O_5$: C, 58.36; H, 4.59; N, 12.76; found: C, 58.81, H, 5.57, N, 12.79; IR (KBr, υ, cm^{-1}): 3381 (w), 1658 (s), 1636 (s), 1517 (s), 1452 (m), 1373 (m), 1306 (s), 1236 (m), 1092 (m), 821 (m), 748 (m), 495 (m). ^{1}H NMR (d_6-DMSO, 400 MHz): δ: 3.66 (m, 2H, CH_2), 3.87 (m, 2H, CH_2), 6.67 (d, 1H, ArH), 6.89 (m, 2H, ArH), 7.40 (m, 1H, ArH), 7.81 (m, 1H, ArH), 8.05 (m, 1H, ArH), 8.41 (s, 1H, CH=N), 9.00 (t, 1H, NH, J = 4 Hz), 12.33 (s, 1H, OH), 14.19 (s, 1H, OH).

H_3L'. Pale solid. Mp 145–146 °C. Analytical data, calc. for $C_{20}H_{25}N_3O_3$: C, 67.58; H, 7.09; N, 11.82; found: C, 67.57, H, 7.07, N, 11.84; IR (KBr, υ, cm^{-1}): 3292 (w), 3081 (w), 2974 (m), 2924 (m), 1656 (s), 1517 (s), 1354 (s), 1267 (s), 1215 (s), 1143 (s), 1010 (s), 954 (w), 864 (w), 761 (m), 648 (m), 603 (m), 594 (m). ^{1}H NMR (d_6-DMSO, 400 MHz): δ: 1.04 (t, 6H, CH_3), 3.29 (m, 4H, CH_2), 3.51 (m, 2H, CH_2), 3.62 (t, 2H, CH_2), 5.90 (d, 1H, ArH), 6.13 (dd, 1H, ArH), 6.84 (m, 2H, ArH), 7.04 (d, 1H, ArH), 7.33 (m, 1H, ArH), 7.79 (dd, 1H, ArH), 8.18 (s, 1H, CH=N), 8.89 (t, 1H, NH).

2.3 Synthesis of EuL and EuL′

General procedure. To a acetonitrile solution of 0.1 mmol H_3L/H_3L', 27 uL (0.2 mmol) triethylamine was added to make a clear solution. Then 0.1 mmol $Eu(NO_3)_3\cdot 6H_2O$ (0.446 mg) was added as a solid, and the solution was stirred for another 4 h to obtain a clear solution which was filtered into a sealed 10–20 mL glass vial for crystallization at room temperature. After

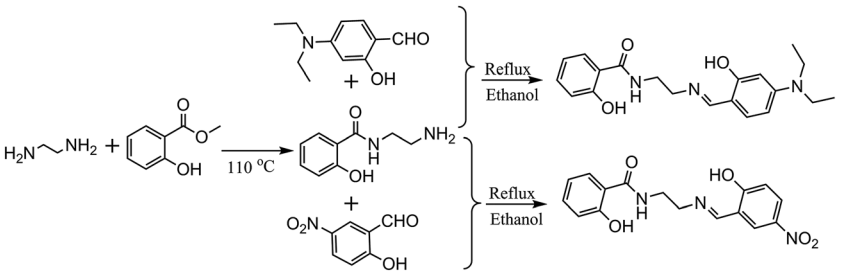

Scheme 1 The synthesis route of the ligand H_3L and H_3L'.

about three weeks, pale yellow single crystals suitable for crystal analysis were obtained and collected by filtration, washed with cold acetonitrile, and dried in the air.

$[Eu_2(H_2L)_3(NO_3)_3]\cdot 3CH_3CN$ (EuL): (yield: 36.7 mg, 52% based on $Eu(NO_3)_3\cdot 6H_2O$). Analytical data (%), calcd: C, 41.47; H, 2.90; N, 11.64; found: C, 41.22; H, 2.88; N, 11.68; IR (KBr, υ, cm^{-1}): 3456 (w), 1606 (s), 1511 (s), 1470 (s), 1446 (s), 1383 (m), 1217 (s), 1168 (s), 1130 (m), 1074 (m), 734 (m), 594 (m).

$[Eu_2(H_2L')_2(NO_3)_4]\cdot 2CH_3CN$ (EuL′): (yield: 37.6 mg, 56% based on $Eu(NO_3)_3\cdot 6H_2O$). Analytical data (%), calcd: C, 39.35; H, 4.05; N, 12.52; found: C, 39.48; H, 4.08; N, 12.50; IR (KBr, υ, cm^{-1}): 3394 (w), 2974 (w), 1602 (s), 1510 (s), 1474 (s), 1308 (m), 1242 (s), 1145 (m), 1012 (m), 816 (m), 741 (m), 584 (m).

2.4 X-ray crystallographic study

Suitable yellow block crystals of EuL (0.21 × 0.16 × 0.12 mm^3) and EuL′ (0.16 × 0.12 × 0. 06 mm^3) were coated with perfluoropolyether oil before mounting. Intensity data were recorded with a Bruker Smart Apex II CCD diffractometer with agraphite-monochromated Mo-Kα radiation (λ = 0.071073 Å) using the ω–2θ scan mode. No crystal decay were observed during the data collections. Absorption corrections based on multi-scan using the SADABS software[14] were applied. The structure was solved by direct methods[15] and refined on F^2 by a full-matrix least-squares procedure based on all data minimizing $w_R = [\Sigma[w(F_o^2 - F_c^2)^2]/\Sigma(F_o^2)^2]^{1/2}$, $R = \Sigma||F_o| - |F_c||/\Sigma|F_o|$ and $S = [\Sigma[w(F_o^2 - F_c^2)^2]/(n-p)]^{1/2}$. SHELXL-2014 was used for both structure solutions and refinements.[16] All non-hydrogen atoms were refined anisotropically. The positions of hydrogen atoms were calculated and isotropically fixed in the final refinement [d(C–H) = 0.95 Å, with the isotropic thermal parameter of Uiso(H) = 1.2 Uiso(C)]. The SMART and SAINT software packages[17] were used for data collection and reduction respectively. Crystallographic diagrams were drawn using the DIAMOND software package.[18] The structures were examined using the Add sym sub routine of PLATON to ensure that no additional symmetry could be applied to the models. Also severely disordered acetonitrile molecules in EuL and EuL′, were removed by SQUEEZE during the structural refinements.[19] For details about the squeezed material, see cif data in ESI.† Therefore, three and one crystalline acetonitrile molecules which were determined on the basis of elemental microanalysis and the data treated with the SQUEEZE routine within PLATON were added to the molecular formula of EuL and EuL′ respectively. A summary of the relevant crystallographic data and the final refinement details are given in Table 1, important bond lengths are listed in Table 2.

Table 1 Crystal data and structure refinement parameters for EuL and EuL′

Empirical formula	$C_{48}H_{42}Eu_2N_{12}O_{24}$	$C_{42}H_{51}Eu_2N_{11}O_{18}$
Crystal system, space group	Trigonal, $R\bar{3}$	Monoclinic, $C2/c$
Unit cell dimensions	a = 17.4511(7) Å, α = 90°	a = 28.3358(12) Å, α = 90°
	b = 17.4511(7) Å, β = 90°	b = 20.1143(7) Å, β = 118.325(4)°
	c = 40.5949(16) Å, γ = 120°	c = 20.98177(7) Å, γ = 120°
Volume	10 706.5(10) $Å^3$	10 526.8(8) $Å^3$
Z, calculated density	6, 1.732 kg m^{-3}	8, 1.643 kg m^{-3}
Absorption coefficient	1.795 mm^{-1}	2.441 mm^{-1}
F(000)	4392	4530
Crystal size	0.21 × 0.16 × 0.12 mm	0.16 × 0.12 × 0.06 mm
Theta range for data collect	3.60 to 25.50°	3.46 to 26.00°
Limiting indices	$-21 \le h \le 11$, $-16 \le k \le 16$, $-49 \le l \le 30$	$-34 \le h \le 33$, $-24 \le k \le 18$, $-25 \le l \le 24$
Reflections collected/unique	7665/4442 [R(int) = 0.0358]	21 725/10 272 [R(int) = 0.0452]
Completeness to theta = 25.01	99.7%	99.2%
Data/restraints/parameters	4442/45/269	10 272/79/672
Goodness-of-fit on F^2	1.036	1.053
Final R indices [I > 2 sigma(I)]	R_1 = 0.0539, wR_2 = 0.1675	R_1 = 0.0514, wR_2 = 0.1221
R indices (all data)	R_1 = 0.0772, wR_2 = 0.1820	R_1 = 0.0780, wR_2 = 0.1388
Largest diff. peak and hole	1.861 and −1.410 e $Å^{-3}$	2.622 and −1.354 e $Å^{-3}$

Table 2 Selected bond lengths (Å) for EuL and EuL′

$[Eu_2(H_2L)_3(NO_3)_3]\cdot 3CH_3CN$ (EuL)				
Eu1–O1 2.311(5) Mn1–O1 1.846(2) Eu2–O2 2.510(5)	Eu1–O7 2.498(6)	Eu1–O6 2.558(5)	Eu2–O3 2.401(5)	Eu2–O1 2.480(4)
$[Eu_2(H_2L')_2(NO_3)_4]\cdot 2CH_3CN$ (EuL′)				
Eu1–O3 2.169(6)	Eu1–O1 2.267(5)	Eu1–O4 2.286(4)	Eu1–O2 2.302(5)	Eu1–O7 2.400(5)
Eu1–O8 2.406(5)	Eu1–O11 2.423(5)	Eu1–O10 2.492(5)	Eu2–O6 2.210(5)	Eu2–O5 2.260(5)
Eu2–O1 2.270(4)	Eu2–O4 2.304(5)	Eu2–O14 2.387(5)	Eu2–O13 2.396(6)	Eu2–O17 2.423(6)
Eu2–O16 2.437(5)				

2.5 Sensing experiment

Luminescence spectra were recorded on a Hitachi F-7000 spectrophotometer. Spectroscopic measurements were recorded in acetonitrile solution. Stock solutions (0.01 M) of the nitrate salts of Li^+, Na^+, Mg^{2+}, Ca^{2+}, Ba^{2+}, Mn^{2+}, Fe^{2+}, Fe^{3+}, Co^{2+}, Ni^{2+}, Cu^{2+}, Cd^{2+}, Hg^{2+}, Zn^{2+} and Al^{3+} in distilled water were prepared. Stock solutions of EuL (0.1 mM) were prepared in acetonitrile solution. Test solutions were prepared by placing 2 mL of the probe stock solution into a test tube and adding an appropriate aliquot of each ions stock. The mixture solution was stirred for 30 seconds, and waited about one minute. Complex formation was monitored following the absorption spectral changes. Both the excitation and emission slit widths were 5.0 and 5.0 nm, respectively.

3 Result and discussion

3.1 Crystal structure of EuL

Signal-crystal X-ray diffraction analysis revealed that EuL is a dinuclear complex with a ligand metal stoichiometric ratio of 3 : 2. As shown in Table 1, EuL crystallizes in the trigonal system space group $R\bar{3}$, which allows a 3-fold rotational axis passes through Eu^{III} ions and thus to give a C_3 molecular symmetry. In the asymmetry unit of EuL, there are two crystallographically independent Eu^{III} ions (Eu1 and Eu2) with one third occupancy, one partly deprotoned H_2L^- and one nitrate anions (Fig. 1a). Eu1 is coordinated by three phenoxy atoms (O1) of salicylamide group from three crystallgraphically equivalent H_2L^- ligands and six oxygen atoms (O6 and O7) from three crystallgraphically equivalent nitrate anions. Meanwhile, Eu2 is coordinated by three amide oxygen atoms (O2), three phenoxy oxygen atoms (O1) and three phenolic hydroxyl atoms (O3) from three crystallgraphically equivalent H_2L^- ligands. Exact geometry analysis by SHAPE 2.1 software shows that the inner coordination sphere of the two nine-coordinated Eu^{III} ions are residing in two distorted tricapped trigonal prism sharing one bottom with a deviation of 13.096 for Eu1 and 12.686 for Eu2 from the ideal *D3h* symmetry (Fig. S1 and Table S1†). The Eu–O bond distances vary from 2.311(5) to 2.558(5) Å and the O–Eu–O bond angles fall in the range of 51.69(5)–158.72(9)°, which are exactly comparable to those reported in other Eu^{III} compounds.[20] As shown in Fig. 1b, the H_2L^- ligands in EuL adopt a chelating-bridging tetradentate μ_4-η_1:η_1:η_2 coordination mode, and as a result, Eu1 and Eu2 ions are linked by three phenoxy atoms (O1) engendering a $[Eu_2(\mu\text{-}O)_3]$ core with a Eu1···Eu2 separation of 3.576 (2) Å and a Eu1–O1–Eu2 angle of 96.46(6)°. Upon further investigation, we find there are hydrogen bonds between imine and phenolic hydroxyl groups with imine groups being hydrogen bonding acceptor and phenolic hydroxyl groups being hydrogen bonding donor. The existence of these intramolecular hydrogen bonds could prevent imine nitrogen atom from coordination. What deserves special note is the preorganized cavity existed in EuL, where the three phenolic hydroxyl groups on 2-(iminomethyl)phenol moiety are arranged in a radial manner anchored with Lewis base sites which can be very useful for binding suitable metal ions.

To confirm the role of different substitution groups in the self-assembly process, H_3L' was used instead of H_3L to perform the reaction under the same experimental conditions. As expected, compound EuL′ crystallizes in the monoclinic *C*2/*c* space group with a 1 : 1 ligand metal stoichiometric ratio which is quite different from that of EuL due to the substitution of nitryl with diethylamino group. A view of the molecular structure with partly numbering scheme is depicted in Fig. 2a. Two crystallographically independent Eu^{III} ions (Eu1 and Eu2), are doubly bridged by two phenoxy of salicylamide with the

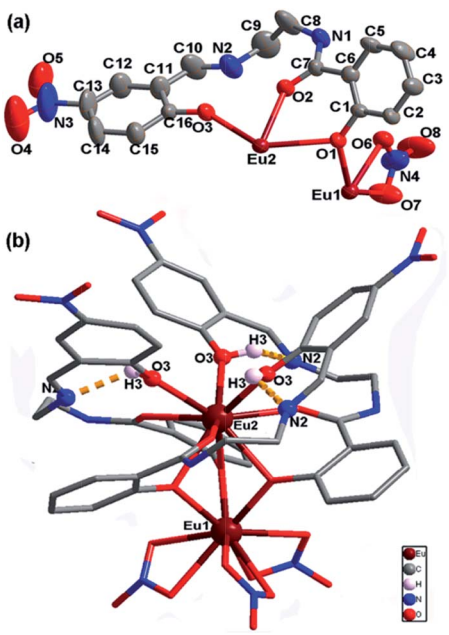

Fig. 1 a) Asymmetric unit of EuL with thermal ellipsoids at 50% probability; (b) molecular structure of EuL showing intramolecular hydrogen bonds between imine and phenolic hydroxyl groups.

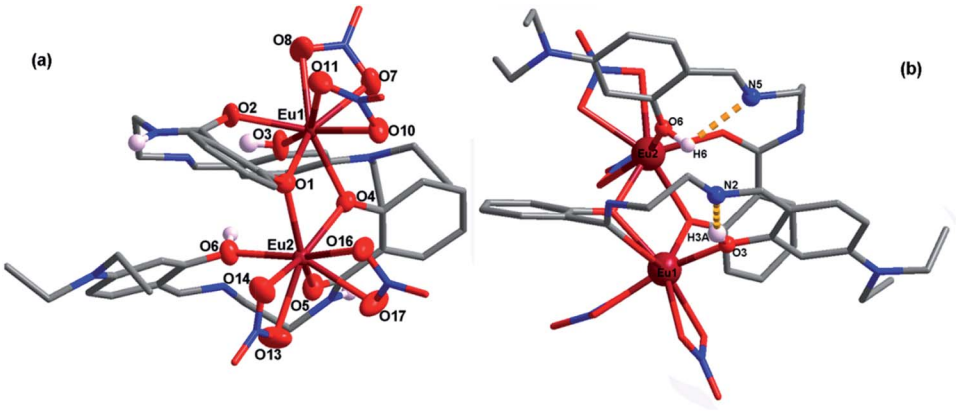

Fig. 2 (a) A view of the molecular structure of EuL′ with partly numbering scheme; (b) molecular structure of EuL′ showing intramolecular hydrogen bonds between imine and phenolic hydroxyl group.

remaining coordinating sites fulfilled by carbonyl oxygen atom, phenolic hydroxy group from the same ligand $H_2L'^-$, and four oxygen atoms from two bidentate nitrate anions. Contrast to Eu^{III} compound of H_3L, two Eu^{III} ions are eight-coordinated and their coordination geometries are distorted square antiprisms sharing one side with a deviation of 5.258 for Eu1 and 7.034 for Eu2 from the ideal D4d symmetry (Fig. S2 and Table S1†) based on exact geometry analysis by SHAPE 2.1 software. Similar to that in EuL, $H_2L'^-$ also adopts tetradentate coordination modes with one phenolic hydroxy group and one amide oxygen atom chelating to one europium ion as well as one phenoxy atom bridging another europium ion. As a result, imine nitrogen atoms were also deprived of coordination due to the existence of molecular hydrogen bonds between imine and phenolic hydroxy groups (Fig. 2b). Notably, the distance of two phenolic hydroxyl groups on 2-(iminomethyl)phenol moiety in EuL′ is 3.847 Å. Clearly, the structural difference between EuL and EuL′ are owing to the electronic property of nitryl and diethylamino group in spite of their poor coordination abilities. Such differences in structure must have an impact on their luminescence sensing ability to metal ions.

3.2. UV-vis absorption studies

The UV-vis titration of Eu^{III} and Al^{3+} were conducted using a 10.0 μM solution of H_3L/H_3L' + triethylamine in CH_3CN. As shown in Fig. 3a and c, the absorption spectrum of H_3L + triethylamine and H_3L' + triethylamine exhibit different absorption properties owing to the different electronic properties of nitryl and diethylamino group: the former shows three strong absorption bands centered at 208, 238 and 252 nm with several relative weak broad bands ranging from 314 to 404 nm which tail out to 450 nm, while the latter exhibits three relatively weak absorption bands centered at 215, 224 and 335. Upon addition of Eu^{III}, there were clearly five isosbestic points at 237, 249, 276, 321 and 403 nm for H_3L + triethylamine, and two isosbestic points at 275 and 348 nm for H_3L' + triethylamine, indicating the formation of the corresponding compound. Obviously, the absorbance of H_3L + triethylamine shows a linear increase until the stoichiometric ratio of Eu^{III} : L reaches 2 : 3, and no longer obvious changes can be observed with continuously titrated of Eu^{III}, suggesting that the stoichiometry between the ligand and Eu^{III} is 3 : 2. Meanwhile, the change observed in Fig. 3c shows a 1 : 1 ligand metal stoichiometric ratio. All these results are consistent with the structural analysis discussed above. Further incremental addition of Al^{3+} to the EuL in CH_3CN, obvious changes in the absorption bands are also observed (Fig. 3b). The absorbance at 232 nm is almost unchanged with concomitant hypsochromic shift in the absorbance at 349 nm and simultaneous development of a new peak at 260 nm. After addition of 1 equiv. of Al^{3+}, saturation point is reached. However, no such significant change in the absorption spectrum of EuL was observed with other tested metal cations. All these may indicate a formation of a complex between EuL and Al^{3+}. By comparision, addition of Al^{3+} to the resulted EuL′ solution bring no spectra change (Fig. 3d), indicating there are no electronic interaction between Al^{3+} and EuL′.

3.3 Luminescence and sensing properties

As shown in Fig. 4, excitation of the absorption bands at 326 nm or 349 nm produce blue fluorescence positioned at 406 and 471 nm for H_3L + NEt_3, and broad emission band at λ_{max} = 406 nm for H_3L' + NEt_3. Upon coordination to Eu^{III} ions, pink emission of EuL and EuL′ were observed by naked eyes following excitation with a standard UV lamp (λ_{ex} = 365 nm). Excitation of the ligand-centered absorption band at 375 nm, emissions both originating from the ligand and Eu^{III} ions were observed with the Eu^{III}-centered emission (619 nm) intensity more than three times higher than that of ligand-centered emissions (432 nm) for EuL for EuL′, confirming that the energy transfers from ligands' chromophore to Eu^{III} ions occur (Fig. 4). The Eu^{III}-centered emissions shows five characteristic bands originated from the $^5D_0$ state to the ^7F_J (J = 0, 1, 2, 3, 4) at about 581, 594, 619, 653 and 698 nm. The first transition ($^5D_0 \rightarrow {}^7F_0$) observed at the wavelength 581 nm is symmetric, indicating only one type of europium were present in all complexes studied.[21] The second transition ($^5D_0 \rightarrow {}^7F_1$) with magnetic dipole nature observed at the wavelength 594 nm. The most intensive maxima correspond to the $^5D_0 \rightarrow {}^7F_2$ transition for

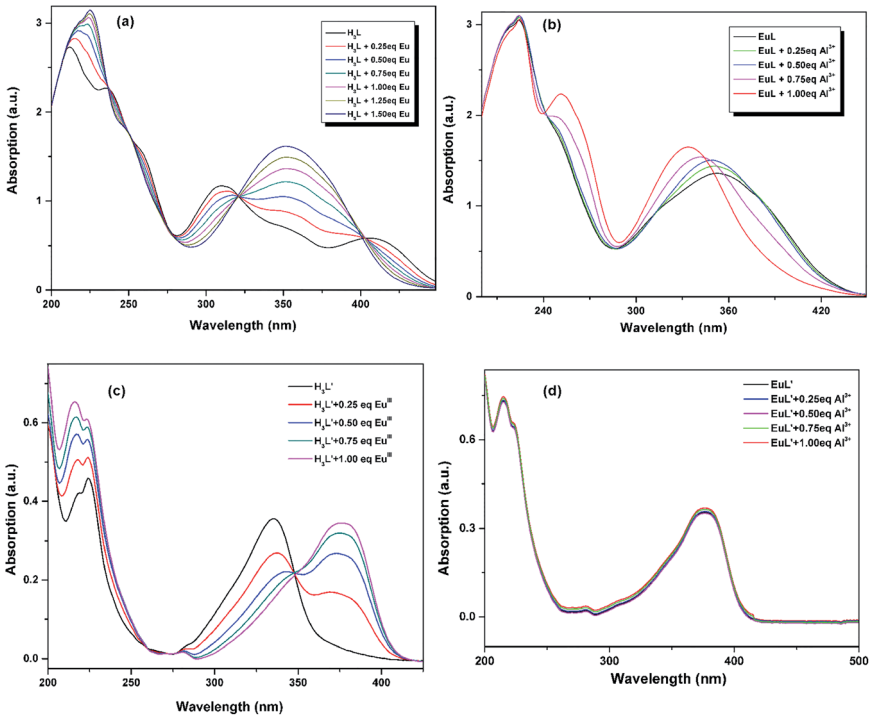

Fig. 3 (a) UV-vis titration of H_3L + triethylamine (10.0 μM) with the addition of increasing concentration of Eu^{III} in CH_3CN; (b) UV-vis titration of EuL (10.0 μM) upon the addition of increasing concentration of Al^{3+} in CH_3CN; (c) UV-vis titration of H_3L' + triethylamine (10.0 μM) upon the addition of increasing concentration of Eu^{III} in CH_3CN; (d) UV-vis titration of EuL′ (10.0 μM) with the addition of increasing concentration of Al^{3+} in CH_3CN.

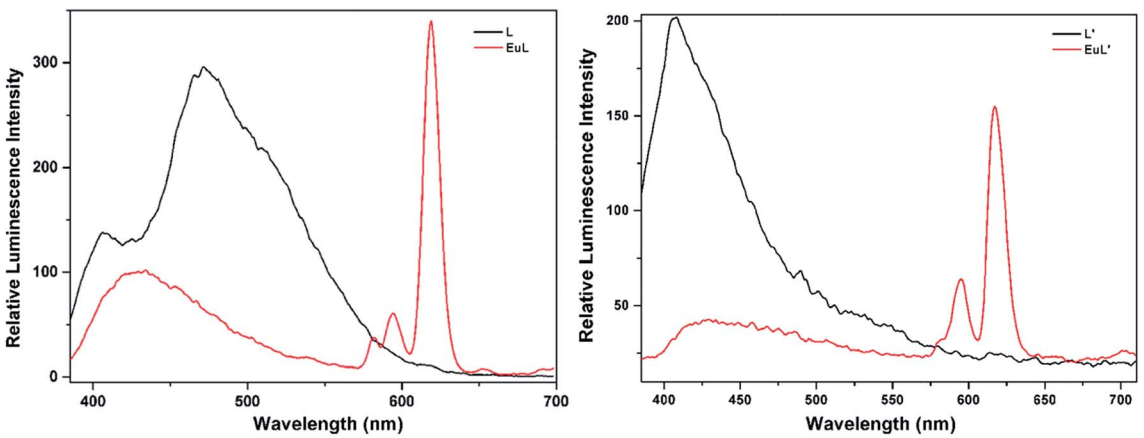

Fig. 4 Emission spectra of H_3L/H_3L' (black solid line) and EuL/EuL′ (red solid line) in CH_3CN.

EuL and EuL′ are found at wavelength 619 nm. The ratios of intensities corresponding to $^5D_0 \rightarrow {}^7F_2$ and $^5D_0 \rightarrow {}^7F_1$ transitions are 5.8 and 2.4 for EuL and EuL′ respectively, showing a strong deviation from central symmetry of Eu^{III} coordination geometry in EuL compared to that in EuL′. The $^5D_0 \rightarrow {}^7F_3$ transition observed at 653 nm is very weak because it is forbidden. It is well-known that the presence of OH oscillators in the lanthanide first coordination sphere provides an efficient non-radiative path.[22] Therefore, owing to the combined effects of excited state intramolecular proton transfer (ESIPT) from phenolic –OH to imine-N and the presence of OH oscillators in the lanthanide first coordination sphere as ascertained by structural analysis, the luminescence of EuL and EuL′ are weak.

The selectivity of EuL and EuL′ towards various common metal ions was examined by addition of 1.0 quiv. aqueous solution containing different metal ions such as Li^+, Na^+, Ca^{2+}, Mg^{2+}, Al^{3+}, Co^{2+}, Fe^{2+}, Ni^{2+}, Fe^{3+}, Mn^{2+}, Cu^{2+} Zn^{2+}, Cd^{2+}, and Hg^{2+} to the solution of EuL and EuL′ in CH_3CN and tested under the same conditions. As depicted in Fig. 5, upon Al^{3+} addition, 5.7 times significant luminescence enhancement was observed for EuL. While for EuL′, a 6.2 times enhancement was caused by Li^+ addition. We can also see from Fig. 5, that transition metal

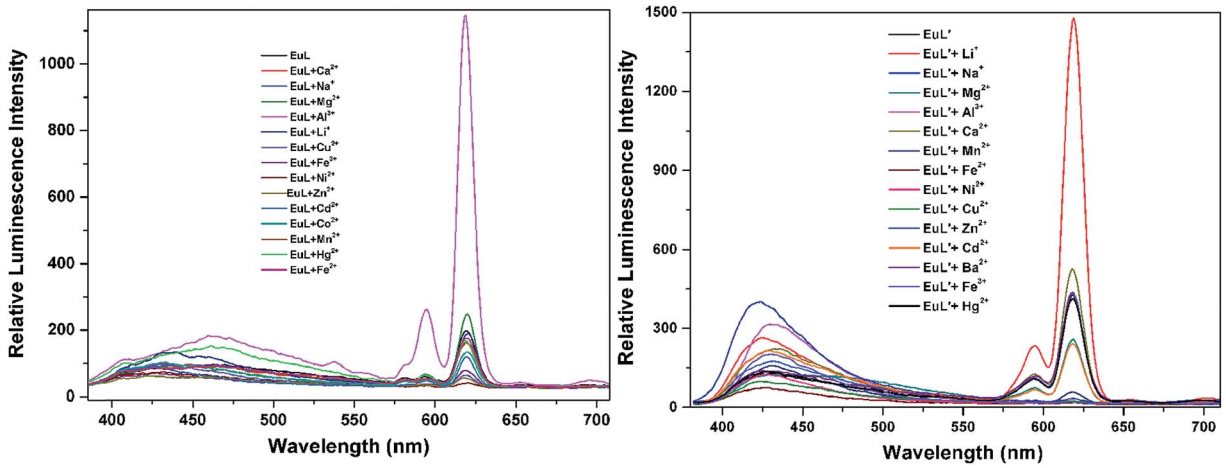

Fig. 5 Comparison of the luminescence intensity of EuL and EuL′ (0.1 mM) upon addition of various metal ions in CH_3CN.

cations with unpaired d-electrons have a little varying degrees quenching effect on the luminescence intensity of EuL and EuL′ as compared to other transition metal with d^{10} electron configuration, alkaline metal ions and alkaline earth metal ions. Furthermore, the considerably 'turn-on' luminescence response of EuL led to the apparent color change from pink to brilliant red which could also be identified by naked eyes easily under UV lamp (Fig. 6).

To explore the effective applications of EuL and EuL′, the luminescence response of EuL towards Al^{3+} and EuL′ towards Li^+ in presence of typical competing ions were studied and the results were shown in Fig. 7. Data in Fig. 7 shows that there is little interference of EuL for detection of Al^{3+} in presence of Li^+, Na^+, Mg^{2+}, Mn^{2+}, Fe^{3+}, Ni^{2+}, Fe^{2+}, Cu^{2+}, Zn^{2+}, Cd^{2+}, Co^{2+} as follows. In the case of Cu^{2+}, quenching of the fluorescence signal was observed. The response of EuL for Al^{3+} detection in the presence of Mn^{2+}, Ni^{2+}, Co^{2+}, Zn^{2+}, Cd^{2+}, and Hg^{2+} is relatively low but clearly detectable. Thus, EuL can be used as a selective luminescent chemosensor for Al^{3+} detection in presence of most competing metal ions. Comparably, very significant interference exists in EuL′ for detecting Li^+ in presence of Mg^{2+}, Mn^{2+}, Fe^{3+}, Ni^{2+}, Fe^{2+}, Cu^{2+}, Zn^{2+}, Cd^{2+}, Co^{2+}, Ca^{2+} and Hg^{2+}. These results clearly indicated that EuL rather than EuL′ could be used as a potential metal-selective luminescent sensor even in presence of a large excess of other competitive metal ions in acetonitrile.

Further determination of sensitivity was carried out by gradually adding Al^{3+} ion aqueous solution to EuL in acetonitrile solution. As shown in Fig. 8, the sequential enhancing of emission intensity at 619 nm of EuL was recorded as a result of gradual increased concentration of Al^{3+} aqueous solution. The emission intensity at 619 nm increases gradually with the increase in concentration of Al^{3+} up to a mole ratio EuL : Al^{3+} = 1 : 1 and then becomes saturated. A luminescence enhancement of 5.7-fold at 619 nm with the quantum yield increasing from $\Phi = 4.5\%$ to $\Phi = 16.9\%$ can be realized upon addition of 1.0 equiv. Al^{3+}. The lifetimes of EuL and its complex with Al^{3+} in acetonitrile were also measured. The lifetime of EuL is quite short (0.16 ms). Upon addition of 1.0 equiv. Al^{3+}, the lifetime of EuL increased to 0.94 ms. Unfortunatly, no crystalline product was obtained upon Al^{3+} addition.

Job's method was further employed to determine the composition of the complex, the luminescence emission intensity of Eu^{III} for complexation between EuL and Al^{3+} has a maximum at a mole fraction of 0.5, thus indicative of the formation of a 1 : 1 complex.[23] (Fig. S3†). As shown in Fig. 9, Benesi–Hiderband plot of $[I_{max} - I_0)/(I - I_0)]$ *vs.* $1/[Al^{3+}]$ gives straight line with slope $K_d = 1.53 \times 10^{-4}$ M with $R^2 = 0.99$, indicating a 1 : 1 moderately strong binding of EuL towards Al^{3+}. This conclusion has also been certified by electrospray ionization mass spectrum (ESI-MS). The positive ion mass spectrum of EuL upon addition of 1.0 equiv. of Al^{3+} exhibited intense peaks at $m/z = 1473.76$ and $m/z = 1642.09$, which can be assigned to the ion of $[EuL - H]^+$, $[EuL - 2H + Al + 3H_2O]^+$ respectively (Fig. S4†). The LOD of Al^{3+} calculated by using 3σ method was found to be 0.33 μM. (Fig. S5†) which is lower than

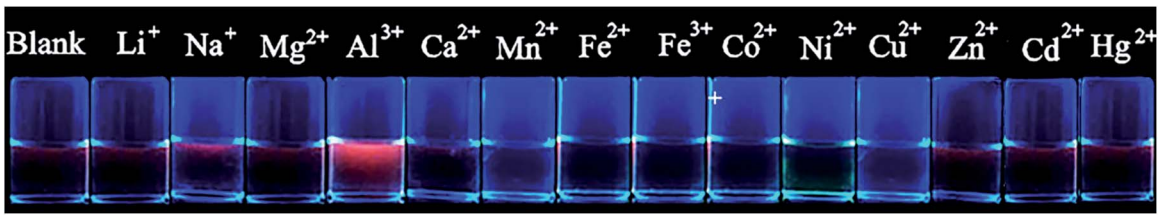

Fig. 6 The visual fluorescence response of EuL (0.1 mM) upon addition of metal ions (0.5 mM) in CH_3CN under UV lamp at 365 nm.

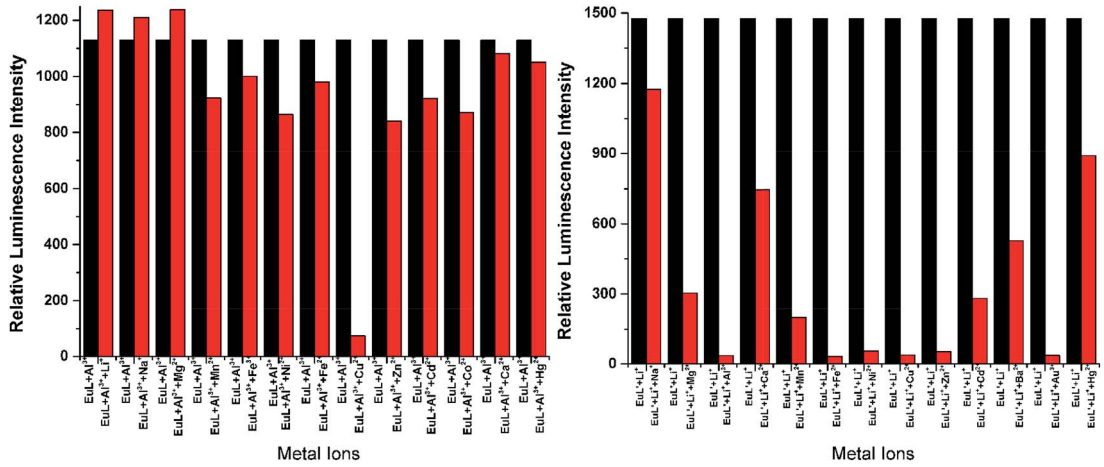

Fig. 7 Bar chart illustrating luminescence response of EuL + Al^{3+} and EuL′ + Li^{+} at 619 nm towards different cations in CH_3CN (λ_{ex} = 375 nm). Conditions: EuL = 0.1 mM, EuL′ = 0.1 mM, Al^{3+} = 0.1 mM, M^{n+} = 0.01 M; where, M^{n+} = Li^{+}, Na^{+}, Mg^{2+}, Mn^{2+}, Fe^{3+}, Ni^{2+}, Fe^{2+}, Zn^{2+}, Cd^{2+}, Co^{2+}, Cu^{2+}, Ca^{2+} and Hg^{2+}.

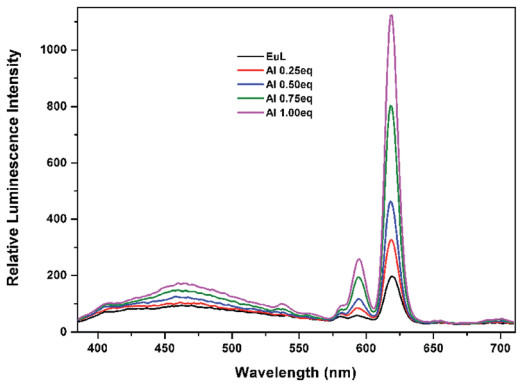

Fig. 8 Luminescence titration spectra of EuL (0.1 mM) upon gradual addition of Al^{3+} (0.1 mM) in CH_3CN (λ_{ex} = 375 nm).

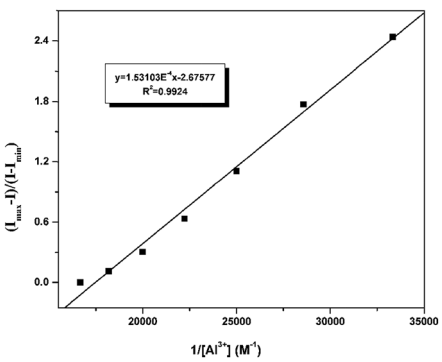

Fig. 9 Benesi–Hiderband plot of EuL toward Al^{3+}.

the maximum tolerable limit of Al^{3+}. Such a low detection limit as well as the selective emission enhancement reach to a conclusion that EuL is an effective sensor for selective detection of Al^{3+} in acetonitrile.

To explore the mechanism of the luminescence turn-on behavior for Al^{3+} ions, we performed HCl titrations where the possibility of the formation of EuL·Al is expected to reduce. For this purpose, 20 μL of 2 M HCl solution was added sequentially to the acetonitrile solution of EuL after addition of 1.0 equiv. Al^{3+} ions. As shown in Fig. 10, the luminescence intensity of Eu^{III} decreased a lot upon gradual addition of HCl, which may be due to the dissociation of EuL·Al as the result of the protonation of phenolic hydroxy group. This strongly supports the state that the interaction between Al^{3+} and EuL is through the formation of EuL·Al at the expense of destroying intra-molecular hydrogen bonding between imine and phenolic hydroxy groups. Therefore, the enhancement of the luminescent intensity of EuL upon Al^{3+} incorporation is presumably due to metal binding to the cavity formed by three phenolic hydroxyl group in EuL followed by excited-state intra-molecular proton transfer (ESIPT) and photo induced electron transfer suppression.

According to the analysis of the structural features, we found that in the molecular structure of EuL, three phenolic hydroxyl groups provide a cavity with hard Lewis base chelating sites together with the geometric uniqueness of the cavity leads to

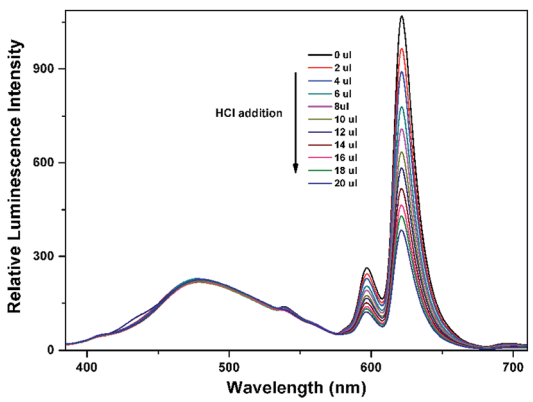

Fig. 10 Concentration-dependent luminescence quenching of compound EuL·Al (0.1 mM) after adding different amounts of 2 M HCl at room temperature.

a high affinity for Al^{3+} (Scheme 2). Among common metal ions examined herein, charge-to-size ratio of Al^{3+} ions is so high that it is expected to destroy the triple intramolecular N···H–O hydrogen bonds in EuL to form EuL·Al, where the three phenolic hydroxy groups of EuL act as simple electron donor to Al^{3+} ions through Lewis acid-base type interactions. Based on the analysis above, Al^{3+} binds to EuL through three hydroxy groups and the hexacoordination of Al^{3+} can be satisfied by three water molecules. Obviously, nitryl groups with strong electron withdrawing effect in EuL plays a key role in constructing this distinctive architecture and the consequent detection of Al^{3+} ion.

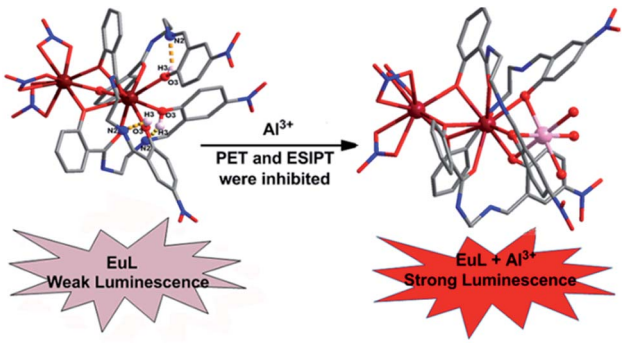

Scheme 2 Sensing mechanism of EuL towards Al^{3+}.

To further understand the relationship between the structure of EuL and the respective optical response to Al^{3+}, we carried out density function theory (DFT) calculations with the B3LYP/6-31 G(d) basis set using the Gaussian 09 program. As displayed in Fig. 11, the HOMO of EuL is distributed on salicylamide moiety of three H_2L^- ligands, meanwhile, the LUMO of EuL is localized on 2-(iminomethyl)phenol moiety, indicating the presence of PET process from salicylamide group of the molecule to the 2-(iminomethyl)-5-nitrophenol moiety. The optimized structure of EuL·Al complex shows that the Al^{3+} ion binds to EuL at phenolic oxygen atoms of 2-(iminomethyl)-5-nitrophenol moiety, with three water molecules to satisfy the need of saturated coordination. In the EuL·Al complex, the electron density of HOMO is also localized on salicylamide moieties, while the electron density of LUMO is localized on the 2-(iminomethyl)-5-nitrophenol moiety. For the electron density as well as energy gap of EuL·Al compared with that of EuL only changed slightly, which excludes the possibility that the increasing of Eu^{III} luminescence is due to a change of the nature of the antenna triplet state. Therefore we can suggest that the observed increase in luminescence intensity, lifetime and quantum yield of the $^5D_0$ level of Eu^{III} is mainly related to the decrease in non-radiative transitions due to the absent of OH oscillators in the Eu^{III} first coordination shell upon Al^{3+} coordination followed by excited-state intra-molecular proton transfer (ESIPT) and photo induced electron transfer suppression.

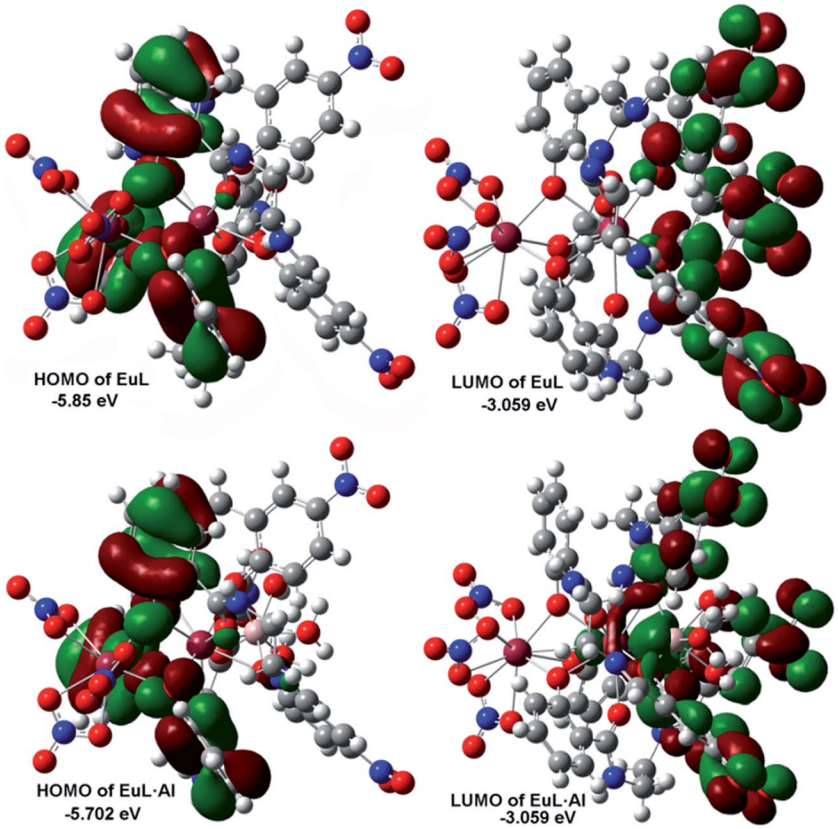

Fig. 11 HOMO–LUMO energy levels and the molecular orbital plots of EuL and EuL·Al.

4 Conclusions

In summary, a novel luminescence-enhanced Eu^{III} complex-supported chemosensor EuL was developed by tuning the substitution group on 2-(iminomethyl)phenol moiety of salicylamide salen-like ligands. The strong electron withdrawing capability of nitryl group led to the formation of the phenoxy bridged dinuclear Eu^{III} complex anchored with Lewis base sites which is distinctive for binding Al^{3+} ions. Its sensing ability for a wide range of metal ions (Li^{+}, Na^{+}, Mg^{2+}, Ca^{2+}, Mn^{2+}, Fe^{2+}, Fe^{3+}, Co^{2+}, Ni^{2+}, Cu^{2+}, Zn^{2+}, Cd^{2+}, Hg^{2+} and Al^{3+}) was tested and the results indicated that EuL exhibited high selectivity and sensitivity for Al^{3+} in the presence of various metal cations. Job's plot and mole–ratio curves revealed a 1 : 1 stoichiometry between EuL and Al^{3+}. To the best of our knowledge, this is the first example of Eu^{III} based luminescent sensor for the detection of Al^{3+} that demonstrated significant luminescence enhancement. The detection limit was sufficiently low to determine the micromolar levels of $Al^{3+}$and EuL could be served as an excellent lanthanide chemsensor for highly toxical aluminum ion. The sensing mechanism can be explained in terms of the decrease of non-radiative transitions in EuL in addition to excited-state intra-molecular proton transfer (ESIPT) and photo-induced electron transfer suppression upon Al^{3+} coordination which is also rationalized by a theoretical calculation. However, EuL is not ideal luminescent sensors for it can't be used in pure aqueous solution.

Acknowledgements

This work was supported by the National Natural Science Foundation of China (Grant 21661019).

Notes and references

1 (*a*) M. Sy, A. Nonat, N. Hildebrandt and L. J. Charbonniére, *Chem. Commun.*, 2016, **52**, 5080; (*b*) A. Foucault-Collet, C. M. Shade, I. Nazarenko, S. Petoud and S. V. Eliseeva, *Angew. Chem.*, 2014, **53**, 2927; (*c*) A. J. Palmer, S. H. Ford, S. J. Butler, T. J. Hawkins, P. J. Hussey, R. Pal, J. W. Walton and D. Parker, *RSC Adv.*, 2014, **4**, 9356; (*d*) A. J. Amoroso and S. J. A. Pope, *Chem. Soc. Rev.*, 2015, **44**, 4723.

2 (*a*) Y. Suffren, D. Zare, S. V. Eliseeva, L. Guenee, H. Nozary, T. Lathion, L. Aboshyan-Sorgho, S. Petoud, A. Hauser and C. Piguet, *J. Phys. Chem. C*, 2013, **117**, 26957; (*b*) S. F. H. Correia, V. de Z. Bermudez, S. J. L. Ribeiro, P. S. André, R. A. S. Ferreira and L. D. Carlos, *J. Mater. Chem. A*, 2014, **2**, 5580; (*c*) J.-C. G. Bunzli and S. V. Eliseeva, *Chem. Sci.*, 2013, **4**, 1939.

3 (*a*) H. Suzuki, *J. Photochem. Photobiol., A*, 2004, **166**, 155; (*b*) Y. Hasegawa and T. Nakanishi, *RSC Adv.*, 2015, **5**, 338; (*c*) S. Z. Zou, Q. P. Li and S. W. Du, *RSC Adv.*, 2015, **5**, 34936; (*d*) H. B. Wei, G. Yu, Z. F. Zhao, Z. W. Liu, Z. Q. Bian and C. H. Huang, *Dalton Trans.*, 2013, **42**, 8951.

4 P. Montgomery, B. S. Murray, E. J. New, R. Pal and D. Parker, *Acc. Chem. Res.*, 2009, **42**, 925.

5 J. C. G. Bünzli, *Chem. Rev.*, 2010, **110**, 2729.

6 (*a*) J. Barcelo and C. Poschenrieder, *Environ. Exp. Bot.*, 2002, **48**, 75; (*b*) B. Valeur and I. Leray, *Chem. Rev.*, 2000, **205**, 3; (*c*) Z. Krejpcio and R. W. P. J. Wojciak, *Environ. Stud.*, 2002, **11**, 251; (*d*) P. Nayak, *Environ. Res.*, 2002, **89**, 111.

7 (*a*) S. Malkondu, *Tetrahedron*, 2014, **70**, 5580; (*b*) A. S. M. Islam, R. Bhowmick, H. Mohammad, A. Katarkar, K. Chaudhuri and M. Ali, *New J. Chem.*, 2016, **40**, 4710; (*c*) D. Maity and T. Govindaraju, *Inorg. Chem.*, 2010, **49**, 7229; (*d*) H. Xu, M. Fang, C. S. Cao, W. Z. Qiao and B. Zhao, *Inorg. Chem.*, 2016, **55**, 4790; (*e*) L. Y. Wang, H. H. Li and D. R. Cao, *Sens. Actuators, B*, 2013, **181**, 749; (*f*) S. H. Kim, H. S. Choi, J. Kim, S. J. Lee, D. T. Quang and J. S. Kim, *Org. Lett.*, 2010, **12**, 560; (*g*) Y. W. Wang, M.-X. Yu, Y.-H. Yu, Z.-P. Bai, Z. Shen, F.-Y. Li and X.-Z. You, *Tetrahedron Lett.*, 2009, **50**, 6169; (*h*) D. Maity and T. Govindaraju, *Chem. Commun.*, 2010, **46**, 4499; (*i*) T. H. Ma, M. Dong, Y. M. Dong, Y. W. Wang and Y. Peng, *Chem.–Eur. J.*, 2010, **16**, 10313; (*j*) Y. S. Kim, G. J. Park, J. J. Lee, S. Y. Lee, S. Y. Lee and C. Kim, *RSC Adv.*, 2015, **5**, 11229.

8 K. Hanaoka, K. Kikuchi, H. Kojima, Y. Urano and T. Nagano, *J. Am. Chem. Soc.*, 2004, **126**, 12470.

9 W. S. Liu, T. Q. Jiao, Y. Z. Li, Q. Z. Liu, M. Y. Tan, H. Wang and L. F. Wang, *J. Am. Chem. Soc.*, 2004, **126**, 2280.

10 A. Thibon and V. C. Pierre, *J. Am. Chem. Soc.*, 2009, **131**, 434.

11 (*a*) N. Shao, J. Y. Jin, G. L. Wang, Y. Zhang, R. H. Yang and J. L. Yuan, *Chem. Commun.*, 2008, **9**, 1127; (*b*) J. W. Wang, J. Wu, Y. M. Chen, H. P. Wang, Y. R. Li, W. S. Liu, H. Tian, T. Zhang, J. Xu and Y. Tang, *Dalton Trans.*, 2012, **41**, 12936; (*c*) C. G. Gulgas and T. M. Reineke, *Inorg. Chem.*, 2008, **47**, 1548; (*d*) M. S. Tremblay, M. Lee and D. Sames, *Org. Lett.*, 2008, **10**, 5; (*e*) H. Akiba, J. Sumaoka, K. Tsumoto and M. Komiyama, *Anal. Chem.*, 2015, **87**, 3834; (*f*) F. Piccinelli, M. Leonzio, M. Bettinelli, M. Monari, C. Grazioli, A. Melchior and M. Tolazzi, *Dalton Trans.*, 2016, **45**, 3310.

12 (*a*) X. Q. Song, G. Q. Cheng, X. R. Wang, W. Y. Xu and P. P. Liu, *Inorg. Chim. Acta*, 2015, **425**, 145; (*b*) X. Q. Song, G. Q. Cheng and Y. A. Liu, *Inorg. Chim. Acta*, 2016, **450**, 386; (*c*) X. Q. Song, Y. K. Lei, X. R. Wang, M. M. Zhao, Y. Q. Peng and G. Q. Cheng, *J. Solid State Chem.*, 2014, **208**, 212.

13 (*a*) P. P. Liu, L. Sheng, X. Q. Song, W. Y. Xu and Y. A. Liu, *Inorg. Chim. Acta*, 2015, **434**, 252; (*b*) X. Q. Song, P. P. Liu, Z. R. Zhou, X. Li and Y. A. Liu, *Inorg. Chim. Acta*, 2015, **438**, 232; (*c*) X. Q. Song, P. P. Liu, Y. A. Liu, J. J. Zhou and X. L. Wang, *Dalton Trans.*, 2016, **45**, 8154.

14 *SADABS, version 2.03*, Bruker AXS Inc, Madison, WI, 2002.

15 G. M. Sheldrick, *Acta Crystallogr., Sect. A: Found. Crystallogr.*, 1990, **46**, 467.

16 G. M. Sheldrick, *SHELXL-2014*, University of Gottingen, Gottingen, Germany, 2014.

17 *SAINT, version 6.02*, Bruker AXS Inc, Madison, WI, 2002.

18 DIAMOND, *Visual Crystal Structure Information System, version 3.1*, Crystal Impact, Bonn, Germany, 2004.

19 A. L. Spek, The calculation of the solvent-accessible was performed by using the PLATON software (similarly herein after), *J. Appl. Crystallogr.*, 2003, **36**, 7.

20 (*a*) K. Norton, T. J. Emge and J. G. Brennan, *Inorg. Chem.*, 2007, **46**, 4060; (*b*) X. Q. Song, L. Wang, M. M. Zhao, G. Q. Cheng, X. R. Wang and Y. Q. Peng, *Inorg. Chim. Acta*, 2013, **408**, 71.

21 N. E. Borisova, A. V. Kharcheva, S. V. Patsaeva, L. A. Korotkov, S. Bakaev, M. D. Reshetova, K. A. Lyssenko, E. V. Belova and B. F. Myasoedov, *Dalton Trans.*, 2017, **46**, 2238.

22 W. D. Horrocks Jr, *J. Am. Chem. Soc.*, 1979, **101**, 334.

23 (*a*) M. Lan, J. Wu, W. Liu, H. Zhang, W. Zhang, X. Zhuang and P. Wang, *Sens. Actuators, B*, 2011, **156**, 332; (*b*) L. Fan, X. H. Jiang, B. D. Wang and Z. Y. Yang, *Sens. Actuators, B*, 2014, **205**, 249.